frontiers | Frontiers in Chemistry

TYPE Original Research
PUBLISHED 30 March 2023
DOI 10.3389/fchem.2023.1156457

OPEN ACCESS

EDITED BY
Nabil Ibrahim,
National Research Centre, Egypt

REVIEWED BY
Yehya Youssef,
National Research Centre, Egypt
Yassine Naciri,
Paris-Saclay University, France

*CORRESPONDENCE
Metin Açıkyıldız,
macikyildiz@kilis.edu.tr

SPECIALTY SECTION
This article was submitted to Green and Sustainable Chemistry, a section of the journal Frontiers in Chemistry

RECEIVED 01 February 2023
ACCEPTED 21 March 2023
PUBLISHED 30 March 2023

CITATION
Açıkyıldız M, Gürses A, Güneş K and Şahin E (2023), Adsorption of textile dyes from aqueous solutions onto clay: Kinetic modelling and equilibrium isotherm analysis.
Front. Chem. 11:1156457.
doi: 10.3389/fchem.2023.1156457

Adsorption of textile dyes from aqueous solutions onto clay: Kinetic modelling and equilibrium isotherm analysis

Metin Açıkyıldız[1]*, Ahmet Gürses[2], Kübra Güneş[2] and Elif Şahin[2]

[1]Advanced Technology Application and Research Center, Kilis 7 Aralık University, Kilis, Türkiye, [2]Department of Chemistry, K. K. Education Faculty, Atatürk University, Erzurum, Türkiye

The commercial activated carbon commonly uses to reduce of dye amount in the textile industry effluents. In this study has focused on the use of a natural clay sample as low cost but potential adsorbent. For this purpose the adsorption of commercial textile dyes, Astrazon Red FBL and Astrazon Blue FGRL, onto clay was investigated. The physicochemical and topographic characteristics of natural clay sample were determined by scanning electron microscopy (SEM), X-Ray fluorescence spectrometry (XRF), X-Ray diffraction (XRD), thermogravimetric analysis (TGA), and cation exchange capacity measurements. It was determined that the major clay mineral was smectite with partial impurities. The effects of several operational parameters such as contact time, initial dye concentration, temperature, and adsorbent dosage on the adsorption process were evaluated. The adsorption kinetics was interpreted with pseudo-first order, pseudo-second order, and intra-particle diffusion models. The equilibrium adsorption data were analyzed using Langmuir, Freundlich, Redlich-Peterson, and Temkin isotherm models. It was determined that the adsorption equilibrium was reached in the first 60 min for each dye. The amount of adsorbed dyes onto clay decreased with increasing temperature, similarly, it decreased with increasing sorbent dosage. The kinetic data were well described by pseudo-second order kinetic model, and adsorption equilibrium data was followed both Langmuir and Redlich-Peterson models for each dyes. The adsorption enthalpy and entropy values were calculated as −10.7 kJ.mol^{-1} and −13.21 J.mol^{-1}.K^{-1} for astrazon red and those for astrazon blue −11.65 kJ.mol^{-1} and 37.4 J.mol^{-1}.K^{-1}, respectively. The experimental results support that the physical interactions between clay particles and dye molecules have an important role for the spontaneous adsorption of textile dyes onto the clay. This study revealed that clay could effectively be used as an alternative adsorbent with high removal percentages of astrazon red and astrazon blue.

KEYWORDS

adsorption, textile dyes, clay, Langmuir isotherm model, pseudo-second order kinetic model

1 Introduction

Many industries such as plastic, leather, textile, food, drug, cosmetics, and paper produce an extensive quantity of the dye-containing effluents in their production processes while the Earth is trying to deal with serious problems such as climate change, global warming, greenhouse effect, loss of biodiversity, and overpopulation. It is known that over ten

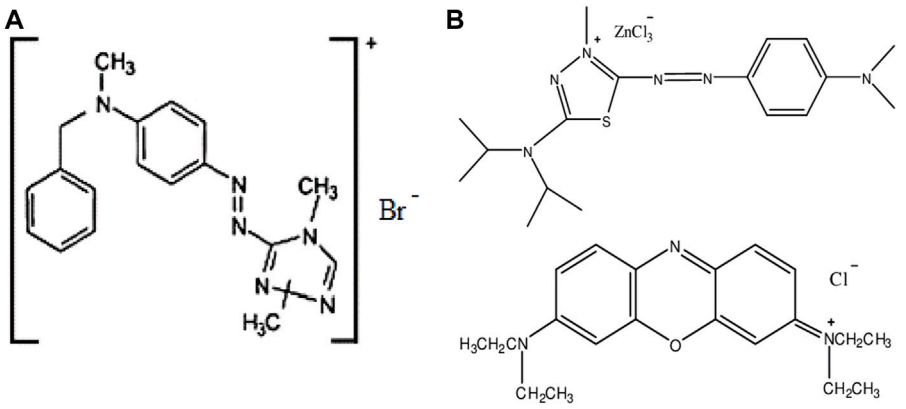

Figure 1
The chemical structures: Astrazon Red **(A)** and Astrazon Blue **(B)**.

thousand different types of dyes and pigments are produced and 700-800 thousand tons of them are used annually in various industries especially in the textile industry around the world (Drumond Chequer et al., 2013; Hussaan et al., 2021). Large amount of water used in the pretreatment, dyeing, printing and finishing stages in the textile industries is polluted with dyes and released into the environment (Hussain and Wahab, 2018; Yaseen and Scholz, 2019). Textile wastewater has very different characteristics in terms of environmental issues such as dark color, wide pH range, high temperature, high chemical and biological oxygen demand (COD and BOD), high concentration of dissolved solids, metal ions and high conductivity (Wang et al., 2022).

The dyestuffs in textile wastewater are considered among the most important pollutants in the aquatic environment due to their complex structure, resistance to biological degradation, and serious effects on water quality, aquatic life, human health and ecosystem. Therefore, it is necessary to constantly monitor the concentration of these pollutants in wastewater and to implement effective and cost-effective treatment methods that ensure their removal from the effluent before it rises above critical values (Jawad and Abdulhameed, 2020; Dehmani et al., 2021; Loutfi et al., 2023). For this aim, the several physical, chemical, and biological methods were developed and used to treat of dye-containing wastewater such as adsorption (Kim et al., 2023), membrane filtration (Zhao et al., 2021), ion exchange (Joseph et al., 2020), photocatalytic degradation (Fu and Ren, 2020), coagulation-flocculation (Ihaddaden et al., 2022), electro-fenton (Jinisha et al., 2018), anodic oxidation (Mo et al., 2020), electrocoagulation (El-Ashtoukhy and Amin, 2010), advanced oxidation (Dadban Shahamat et al., 2022), reverse osmosis (Nataraj et al., 2009), enzyme (Riegas-Villalobos et al., 2020), bacteria (Srinivasan et al., 2022), yeast (Martorell et al., 2012), fungal (Gul et al., 2023), and algae (Zhang et al., 2022) assisted degradation (Al-Tohamy et al., 2022).

All of these methods have various advantages but they also have disadvantages such as high operating and maintenance costs, to cause secondary pollution with using large quantities of chemicals and producing sludge wastes (Gupta et al., 2001; Açıkyıldız et al., 2015). The adsorption process, which still maintains its value as an effective and well-known method in color removal from wastewaters, has superior properties compared to other methods in terms of high efficiency, low cost, low energy requirement, design flexibility, and ease of application (Rápó and Tonk, 2021; Gul et al., 2022). The commercial activated carbon is commonly utilized as an effective adsorbent in the adsorption process but researches are still carried out for organic or inorganic cheap and effective alternatives due to its high production and regeneration costs (Arellano-Cardenas et al., 2013; Abidi et al., 2015). Recently developed polymeric (Naciri et al., 2022) and metallic composites (Tanji et al., 2021) have been proposed as effective alternatives for the adsorption (Imgharn et al., 2022) or photocatalytic degradation (Fahoul et al., 2022) of metal ions (Imgharn et al., 2023), dyes (Hsini et al., 2021), and other organic pollutants. However, clay minerals have been mostly used to remove dyes from aqueous solutions (Bhattacharyya et al., 2014) since their properties such as non-toxicity, naturally abundancy, low-cost, high surface area, and porosity (Gürses et al., 2009). But, there are very few studies in the literature on the removal of astrazon red and astrazon blue, which are widely used in the textile industry, by adsorption on the clay surface.

This study aims to study the adsorption of two commercial textile dyes, astrazon red and astrazon blue, from aqueous environment onto natural clay. In addition, the study exhibits kinetic modeling and equilibrium isotherm analysis as well as the primary data on the effect of various experimental parameters such as initial dye concentration, sorption contact time, temperature, and sorbent dosage.

2 Experimental

The natural clay used as adsorbent was collected from the Kilis region in Turkey. The purification of the raw clay was carried out by decantation. The suspension was dried at 105°C for 24 h in an oven and then solid samples were milled and sieved to obtain a below 106 μm size fraction. The physicochemical and topographic properties of natural clay sample were determined by scanning

TABLE 1 Chemical composition of clay sample.

Constituent	%
SiO_2	41.64
Al_2O_3	8.32
MgO	7.11
Fe_2O_3	5.83
CaO	4.06
Na_2O	1.00
K_2O	0.73
Loss of ignition	27.84

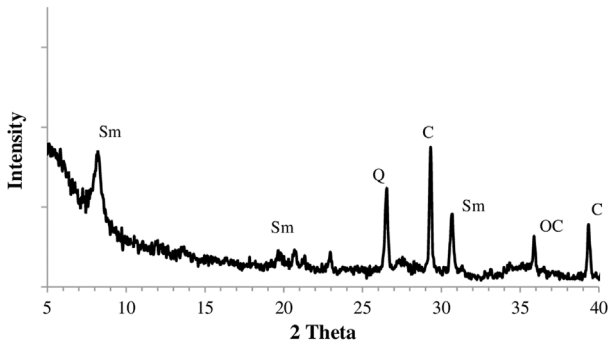

Figure 2
The X-Ray diffractogram of natural clay sample (Sm: Smektit, Q: Quartz, C: Calcite, OC: Opal-C).

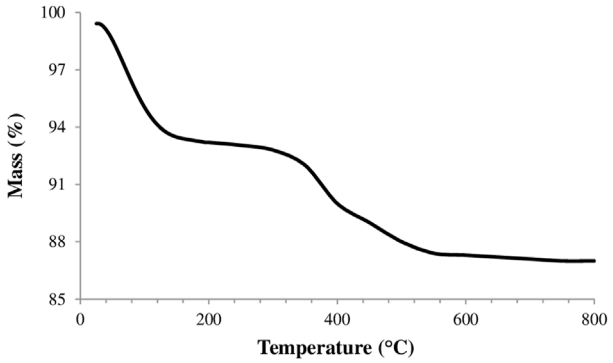

Figure 3
TGA thermogram of natural clay sample.

electron microscopy (SEM), X-Ray fluorescence spectrometry (XRF), X-Ray diffraction (XRD), thermogravimetric analysis (TGA), and cation exchange capacity measurements.

As adsorbate commercial textile dyes, Astrazon Red FBL (AR) and Astrazon Blue FGRL (AB), were chosen. Astrazon Red FBL (C.I. Basic Red 46) is a cationic dyestuff and its formula is $C_{18}H_{21}N_6Br$. Astrazon Blue FGRL is a cationic dye consists of two main components, which are C.I. Basic Blue 159 ($C_{17}H_{27}Cl_3N_6SZn$) and C.I. Basic Blue 3 ($C_{20}H_{26}ClN_3O$). The ratio of the two components is 5:1 by weight, respectively. Though astrazon blue is a mixture of two basic components the following sections will consider it as a single dye species. The dyes were supplied from a textile factory in Gaziantep (Türkiye) and were of commercial quality. Their chemical structures are shown in Figure 1.

Adsorption experiments were carried out in 100 mL glass flasks immersed in a thermostatic shaker. Instead of comparing the adsorptive behavior of the two dyes under the same conditions, different experimental conditions were used for the two dyes, taking into account the findings obtained from the preliminary experiments, in order to meet the equilibrium conditions of dye adsorption for both dyes. A certain amount of clay sample (0.20 g for astrazon red and 0.15 g for astrazon blue) was added to 100 mL of the aqueous dye solutions of the different initial concentrations (20, 40, 60, 80, and 100 $mg.L^{-1}$ for astrazon red, 25, 50, 75, 100, and 125 $mg.L^{-1}$ for astrazon blue). The flasks with its contents were then shaken for the different adsorption times (15, 30, 60, 120, 240 min for astrazon red, 30, 60, 120, 180, and 240 min for astrazon blue) at 293, 313, and 333 K at constant stirring speed (130 min^{-1}). At the end of adsorption period, the supernatant was centrifuged for 4 min at 3,500 min^{-1}. The concentration of astrazon red and astrazon blue in the supernatant solution was calculated by using UV-Vis spectrophotometer (Biocrome Libra S70) at 531 and 601 nm, respectively. The adsorbed dye amount ($mg.g^{-1}$) per gram of clay was calculated by considering the difference between the initial and final concentrations of the solutions.

3 Results and discussion

3.1 Adsorbent characterization

The chemical composition of the clay sample determined by X-ray fluorescence spectrometry (Rigaku RIX-3000) was presented in Table 1.

The crystallographic analysis of the natural clay sample was performed using an X-ray Diffractometer (Philips X'Pert Pro) with a CuK_α (1.540 Å) radiation over a 2θ range of 2°–40° with 2°/min the scanning rate (Figure 2). It was determined from XRD results; the major clay mineral was smectite in the natural clay sample. In addition XRD patterns presented that natural clay sample still contained quartz, calcite, and opal-C as non-clay minerals (Önal and Sarıkaya, 2007). This is also consistent with the XRF findings presented in Table 1.

Thermogravimetric analysis (TGA) of clay sample was carried out using a thermogravimetric analyzer (Shimadzu DTG 60H) at a temperature range of 25°C–800°C and the obtained thermogram was presented in Figure 3. It can be seen from this figure the decomposition of natural clay evolved in two steps.

The first step is observed before 200°C with 6.2% mass loss. It is attributed to the dehydration of physically adsorbed water and water molecules around the exchangeable metal cations in the clay interlayers. The second step occurring with 4.8% mass loss over 350°C was attributed to the loss of dehydroxylation of the structural OH units of the clay (Önal and Sarıkaya, 2007). The topography and

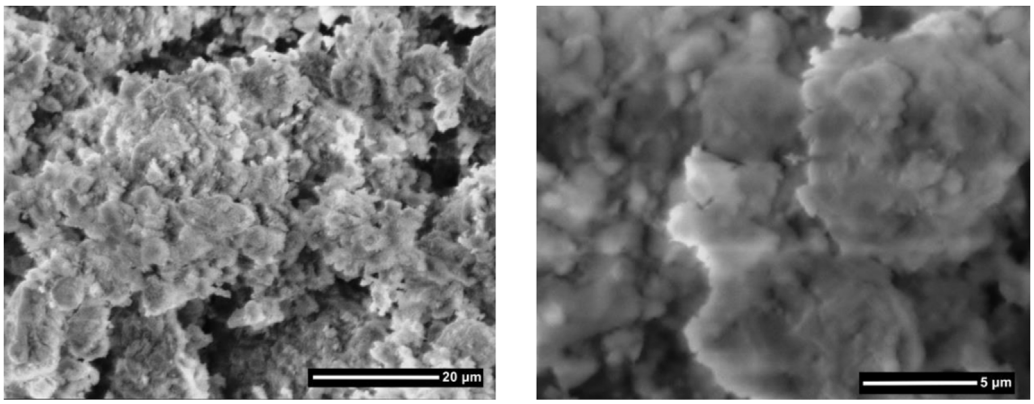

Figure 4
The SEM images of clay sample.

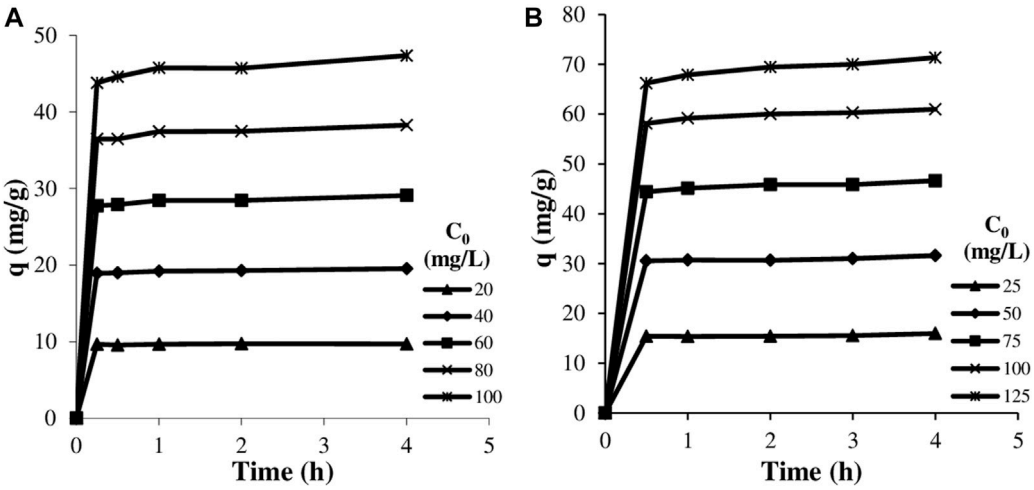

Figure 5
The variation of the amount adsorbed with adsorption time at various initial dye concentrations: astrazon red **(A)** and astrazon blue **(B)**.

morphology of the clay sample was observed by FE-SEM (Zeiss, Supra 55) and the obtained SEM images were shown in Figure 4. The cation exchange capacity (CEC) of clay sample which determined the ammonium acetate method was 63 meq per 100 g clay (Gürses et al., 2009). The observed porous structure and the measured partially high cation exchange capacity offer the clay sample as a potential adsorbent.

3.2 The effect of initial dye concentration and contact time

The effect of initial concentration (20–100 mg.L^{-1} for astrazon red, 25–125 mg.L^{-1} for astrazon blue) on adsorption of the textile dyes onto clay at different times (15, 30, 60, 120, 240 min for astrazon red, 30, 60, 120, 180, and 240 min for astrazon blue) at 293 K was investigated. The results are given in Figures 5A, B.

As seen from these figures, while the initial dye concentration increased, the amount of adsorbed dye increased as expected. This situation can be explained by the concentration difference, which is the driving force in the adsorption of the dye from the solution to the clay surface. It is also seen that the amount of dye adsorbed for both dyes increases significantly up to 30–60 min and remains almost constant after this time. The high adsorption rate emphasizes the physical character of the adsorption process and evokes strong electrostatic interactions between cationic dye molecules and the negatively charged clay particles. However, due to partial differences especially at high concentrations, the adsorption equilibrium time was accepted as 60 min for subsequent experiments.

The fitting of the experimental kinetic data to the pseudo-first-order, pseudo-second-order, and intra-particle diffusion models was

TABLE 2 Kinetic values calculated for adsorption of the textile dyes onto clay.

Dyes	C_{init} (mg.L^{-1})	Pseudo-first order			Pseudo-second order				Intra-particle diffusion		
		$q_{e,cal}$ (mg.g^{-1})	k_1x10^{-3} (min^{-1})	R^2	$q_{e,cal}$ (mg.g^{-1})	$q_{e,\ exp}$ (mg.g^{-1})	k_2 (g.mg^{-1}.min^{-1})	R^2	C	k_i x10^{-2} (mg.min$^{-1/2}$.g^{-1})	R^2
Astrazon red	20	0.112	20.09	0.655	9.699	9.690	0.377	1.000	9.57	0.84	0.375
	40	0.674	8.71	0.902	19.569	19.538	0.049	1.000	18.724	5.29	0.967
	60	1.362	7.16	0.735	29.155	29.068	0.022	0.999	27.328	11.14	0.938
	80	1.971	8.58	0.764	38.462	38.259	0.016	0.999	35.829	15.85	0.919
	100	3.360	7.08	0.698	47.619	47.342	0.009	0.999	42.992	27.98	0.925
Astrazon blue	25	0.636	2.22	0.710	15.974	15.963	0.024	0.999	15.035	4.84	0.657
	50	1.205	3.36	0.813	31.646	31.622	0.014	0.999	29.925	9.30	0.768
	75	2.503	7.37	0.881	46.948	46.645	0.009	0.999	43.369	20.66	0.949
	100	3.440	9.58	0.973	61.349	60.978	0.008	0.999	56.893	26.61	0.966
	125	6.165	8.81	0.973	71.942	71.363	0.004	0.999	63.878	48.10	0.976

10.3389/fchem.2023.1156457

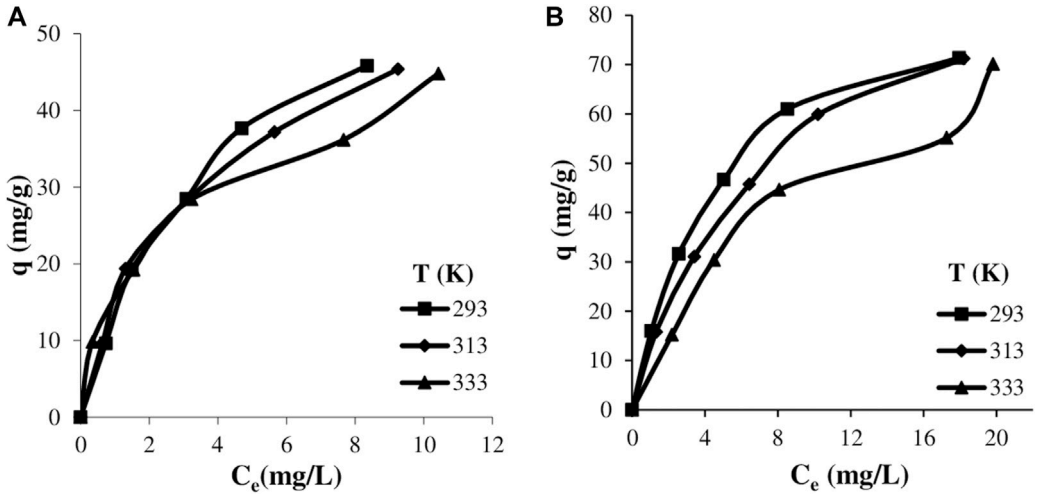

Figure 6
The variation of the amount adsorbed with equilibrium dye concentration for various temperatures: astrazon red **(A)** and astrazon blue **(B)**.

TABLE 3 The thermodynamic quantities calculated for adsorption systems.

Temperature (K)	Astrazon red			Astrazon blue		
	ΔG_{ads} (kJ.mol^{-1})	ΔH_{ads} (kJ.mol^{-1})	ΔS_{ads} (J.mol^{-1}K^{-1})	ΔG_{ads} (kJ.mol^{-1})	ΔH_{ads} (kJ.mol^{-1})	ΔS_{ads} (J.mol^{-1}K^{-1})
293	−6.83	−10.7	−13.21	−22.61	−11.65	37.40
313	−6.57			−23.36		
333	−6.30			−24.10		

investigated in order to decide the adsorption mechanism of both dyes. The linear forms of pseudo-first order, pseudo-second order, and intra-particle diffusion model given in respectively below (Eqs 1–3) were used to calculate kinetic parameters:

$$\ln(q_e - q_t) = ln\, q_e - k_1 t \quad (1)$$

$$\frac{t}{q_t} = \frac{1}{k_2 q_e^2} + \frac{t}{q_e} \quad (2)$$

$$q_t = k_i t^{1/2} + C \quad (3)$$

where, q_t is the amount of dye adsorbed at time t (mg.g^{-1}), q_e is the adsorbed amount of dye at equilibrium, k_1, k_2, and k_i are the rate constants and C is a constant proportional to the boundary layer thickness (Gürses et al., 2006). The calculated kinetic values and fitting parameters for each kinetic model were presented in Table 2.

From Table 2, it can be seen that the experimental data have the highest fit to the second-order kinetic model. This very high agreement indicates that the adsorption takes place through strong electrostatic interactions, H-bonding and, n-π interactions. It can be said that the electrostatic interactions occur between the dye cations and the negatively charged surface, the H-bonding occurs between the H atoms on the clay surface and the N atoms in the dye molecules, and the n-π interactions occur between the lone pair electrons of the O atoms on the clay surface and the π orbitals in the aromatic dye chains (Gamoudi and Srasra, 2019; Jawad and Abdulhameed, 2020). In addition, the isotherm analysis results suggesting monolayer adsorption also supports this assessment. It can be seen that the rate constants calculated for astrazon red are higher than the rate constants calculated for astrazon blue when examining the data presented in Table 2 for the second-order kinetic model. This difference can be explained by the fact that relatively smaller astrazon red molecules diffuse faster from the solution to the adsorbent surface and then into the pores.

3.3 The effect of temperature

The effect of temperature on the adsorption of textile dyes onto clay was studied for the various initial dye concentrations at 293, 313, and 333 K. The experimental results are presented in Figures 6A, B, respectively.

It is seen from these figures that the isotherms are similar to the Type I isotherm especially at low and medium temperatures, that is, the amount of adsorbed dye increases significantly at low equilibrium concentrations, and then increases with lower slope as the equilibrium concentration increases, reflecting the formation of a plateau. It can be said that the isotherm obtained from the experiments carried out at 333 K is similar to the Type II isotherm, and after a plateau below the monolayer capacity formed at 293 and

TABLE 4 Constant parameters and correlation coefficients calculated for various adsorption models.

Isotherm equations	Dye	Constant parameters		R^2
Freundlich	Astrazon Red	n = 0.610	k = 13.37	0.985
$\ln q = \ln k + n \ln C$	Astrazon Blue	n = 0.537	k = 17.60	0.955
Langmuir	Astrazon Red	q_m = 67.11	K = 0.246	0.998
$\frac{C}{q} = \frac{1}{Kq_m} + \frac{1}{q_m} C$	Astrazon Blue	q_m = 90.91	K = 0.210	0.998
Redlich-Peterson	Astrazon Red	g = 0.986	B = 0.272	0.998
$\ln (A \frac{C_e}{q_e} - 1) = g \ln (C_e) + \ln (B)$	Astrazon Blue	g = 0.982	B = 0.204	0.998
Temkin	Astrazon Red	K_T = 14.18	a_T = 2.66	0.989
$q_e = K_T (\ln a_T) + K_T (\ln C_e)$	Astrazon Blue	K_T = 20.30	a_T = 2.02	0.992

TABLE 5 The monolayer adsorption capacities of some adsorbents for astrazon blue and astrazon red adsorption.

Adsorbent	Adsorbate	q_m (mg.g^{-1})	Ref
Fungal (*Funalia trogii*) pellets	Astrazon red	42.24	Yesilada et al. (2002)
Coal mining wastes	Astrazon red	45.90	Almeida et al. (2010)
Posidonia oceanica L. leaves	Astrazon red	68.97	Cengiz et al. (2012)
Sepiolite	Astrazon red	106.0	Santos and Boaventura (2008)
Vermiculite	Astrazon red	44.00	Stawiński et al. (2017)
Acid treated vermiculite		64.00	
Base treated vermiculite		155.0	
Sepiolite	Astrazon blue	155.5	Karagozoglu et al. (2007)
Fly ash		128.2	
Activated carbon		181.5	
Chitosan/polypropenoic acid/ethylenediamine/magnetite nanocomposite hydrogel	Astrazon blue	194.1	Ali et al. (2022)
Macroalga (*Caulerpa lentillifera*)	Astrazon blue	30.67	Marungrueng and Pavasant (2006)
		80.70	Pimol et al. (2008)
Clay	Astrazon red	67.11	This study
	Astrazon blue	90.91	

313 K, the second layer begins to form at high equilibrium concentrations. When the isotherms are examined in general, it can be seen from Figures 6A, B that the adsorption process has an exothermic nature and the amount of adsorbed dye partially decreases as the temperature increases.

Thermodynamic parameters such as isosteric adsorption enthalpy (ΔH), isosteric adsorption entropy, and standard free energy change of adsorption were calculated by considering of the following equations (Doğar et al., 2010):

$$\frac{d\ (lnC)}{d\ (1/T)} = \frac{-(\Delta H_{ads})}{R} \quad (4)$$

$$\frac{d\ (lnC)}{d\ (\ln T)} = \frac{\Delta S_{ads}}{R} \quad (5)$$

$$\Delta G^0_{ads} = \Delta H_{ads} - T.\Delta S_{ads} \quad (6)$$

where, C is the equilibrium dye concentration in different temperatures, T is the absolute temperature, and R is gas constant (J.mol^{-1}.K^{-1}), respectively.

These calculations were based on the same amount of adsorbed dye at different temperatures corresponding to different equilibrium dye concentrations in which adsorption efficiencies were almost the highest (Doğar et al., 2010). The calculated thermodynamic parameters are given in Table 3. The calculated negative values of isosteric enthalpy and free energy changes for both dyes indicate that the adsorption process is spontaneous and exothermic (Brini et al., 2021). It can also be seen from this table that the calculated isosteric adsorption entropy changes for both ionic dye adsorptions

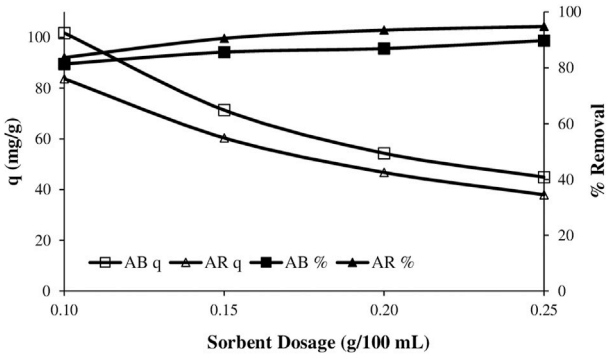

Figure 7
The variation of the amount adsorbed and the removal percentage with sorbent dosage.

are relatively small and of opposite sign. This can be related to the molecular sizes and degree of hydration of the dyes. It is expected that the adsorption entropy is negative as with astrazon red. In the adsorption of astrazon blue, which has more hydrophilic groups, it can be said that the increase in entropy becomes more dominant as a result of the increase in the degree of freedom of the hydrated water layers after the adsorption of the dye molecules. Depending on the change in Gibbs free energies, the tendency to be spontaneous of adsorption decreases for astrazon red and increases for astrazon blue while temperature increases. This is consistent with the exothermic adsorption process and the sign of entropy changes.

3.4 Adsorption isotherms

In order to determine the mechanism of astrazon red and astrazon blue adsorption the experimental data were applied to Freundlich, Langmuir, Redlich-Peterson, and Temkin isotherm equations. The parameters and correlation coefficients calculated for the models are given in Table 4 together with the isotherm equations.

In these equations; C_e is the equilibrium dye concentration ($mg.L^{-1}$), q_m is the maximum adsorption capacity ($mg.g^{-1}$), q_e is the amount of adsorbed dye at equilibrium ($mg.g^{-1}$), k is the Freundlich constant (adsorption intensity), 1/n is the order of adsorption, K is the Langmuir constant related to the energy or net enthalpy of adsorption, A, B and g are the Redlich-Peterson isotherm constants, a_T is Temkin isotherm equilibrium binding constant ($L.g^{-1}$), K_T is constant related to heat of sorption ($J.mol^{-1}$).

High agreement with the Langmuir and Redlich-Peterson (R-P) models observed for each dye is very important. The Redlich-Peterson (R-P) isotherm is a three-parameter empirical adsorption, both from Langmuir and Freundlich isotherms cover the relevant terms and can compensate for their existing shortcomings. Although the high fit with the Langmuir model implies that dye adsorption is limited to the monolayer, the observed fit with the Redlich-Peterson (R-P) isotherm also suggests that this coating is not necessarily ideal, and the homogeneity of the surface in terms of functional groups does not indicate that there is no lateral interaction between the adsorbed species. Accordingly, considering the layered structure of the clay, it can be claimed that both cationic dye ions are replaced by exchangeable cations in the interlayer region by the ion-exchange mechanism.

The high fit to the Langmuir model for each dye suggests that the clay surface is relatively homogeneous in terms of functional groups, dye adsorption onto clay is limited with a monolayer, and there is no significant interaction among adsorbed species. This high fitting also signs that the adsorption occurs predominantly through electrostatic interactions between dye cations and negatively charged clay surface (Gürses et al., 2004; Jawad and Abdulhameed, 2020).

The monolayer adsorption capacities determined from the Langmuir isotherm were compared with the maximum adsorption capacities reached in studies carried out under similar conditions for the removal of astrazon blue and astrazon red from aqueous solution (Table 5).

When Table 5 is examined, it is seen that the monolayer adsorption capacities calculated for natural clay sample used in this study are above the average values for both dyes compared to other adsorbents used in the literature.

3.5 Effects of sorbent dosage

The effect of adsorbent dosage was studied at 293 K, for 60 min, and initial dye concentration of 100 $mg.L^{-1}$ and 125 $mg.L^{-1}$ for astrazon red and astrazon blue respectively. The adsorbed amount of dyes decreased with increasing adsorbent dosage as expected. While dye removal (%) increased up 0.15 g and then it almost remains constant or slightly increased for each dye (see Figure 7).

The tendency of the adsorbed dye amounts to decrease against the adsorbent dosage can be explained that the increase in the amount of adsorbent does not mean that the active sites available for adsorption also increase proportionally, that higher amount of the adsorbent cause partial aggregation. In addition, this situation can be attributed that the unsaturation of the sites responsible for the adsorption process (Brini et al., 2021). The relatively increasing trend of removal ratios against adsorbent dosage also supports this claim. That is, although not proportional to the increase in amount, increasing adsorbent dosage led to a certain increase in dye uptake (Doğar et al., 2010).

4 Conclusion

In this study, the adsorption of cationic dyes Astrazon Red FBL and Astrazon Blue FGRL on clay was investigated. A purified natural clay sample which was characterized by XRD, XRF, and TGA analyzes has been used in the adsorption experiments. The effect of process parameters such as initial dye concentration, contact time, temperature, and solid/liquid ratio were examined for adsorption efficiency.

As a result of the findings obtained from these experiments:

- When initial dye concentration increases, the amount of the adsorbed dye increases as expected,
- The adsorption equilibrium is reached for both dyes in very low adsorption times. It was found that 60 min is sufficient in order to reach adsorption equilibrium for each dye.
- The pseudo-second order model provided the best fit to the kinetic data among the investigated kinetic models.
- The adsorption isotherms are similar to the Type I isotherm, especially at low and medium temperatures; at high temperatures, the isotherms in part suggest that the Type II isotherm and the second adsorbed layer begins to form especially at high equilibrium concentrations,
- Equilibrium data fit well to Langmuir and Redlich-Peterson models for each dyes
- The calculated Gibbs free energy and enthalpy changes are negative,
- It has been determined that adsorption has exothermic nature and entropy decreases for Astrazon Red adsorption and entropy increases for Astrazon Blue adsorption.

As a result, it was determined that the natural clay sample could be used as an alternative adsorbent with a high removal ratio of 95% for Astrazon Red and 90% for Astrazon Blue.

Data availability statement

The raw data supporting the conclusion of this article will be made available by the authors, without undue reservation.

Author contributions

MA: Investigation, conceptualization, methodology, software, validation, writing- original draft preparation. AG: Supervision, conceptualization, methodology, writing- original draft preparation. KG: Formal analysis, visualization, writing- reviewing and editing EŞ: Formal analysis, visualization, writing- reviewing and editing.

Acknowledgments

The authors would like to thank F. Polat and M. Ozhallac for technical support to experiments.

Conflict of interest

The authors declare that the research was conducted in the absence of any commercial or financial relationships that could be construed as a potential conflict of interest.

Publisher's note

All claims expressed in this article are solely those of the authors and do not necessarily represent those of their affiliated organizations, or those of the publisher, the editors and the reviewers. Any product that may be evaluated in this article, or claim that may be made by its manufacturer, is not guaranteed or endorsed by the publisher.

References

Abidi, N., Errais, E., Duplay, J., Berez, A., Jrad, A., Schafer, G., et al. (2015). Treatment of dye-containing effluent by natural clay. *J. Clean. Prod.* 86, 432–440. doi:10.1016/j.jclepro.2014.08.043

Açıkyıldız, M., Gürses, A., Güneş, K., and Yalvaç, D. (2015). A comparative examination of the adsorption mechanism of an anionic textile dye (RBY 3GL) onto the powdered activated carbon (PAC) using various the isotherm models and kinetics equations with linear and non-linear methods. *Appl. Surf. Sci.* 354, 279–284. doi:10.1016/j.apsusc.2015.07.021

Al-Tohamy, R., Ali, S. S., Li, F., Okasha, K. M., Mahmoud, Y. A.-G., Elsamahy, T., et al. (2022). A critical review on the treatment of dye-containing wastewater: Ecotoxicological and health concerns of textile dyes and possible remediation approaches for environmental safety. *Ecotoxicol. Environ. Saf.* 231, 113160. doi:10.1016/j.ecoenv.2021.113160

Ali, H. E., Nasef, S. M., and Gad, Y. H. (2022). Remediation of Astrazon blue and Lerui acid brilliant blue dyes from waste solutions using amphoteric superparamagnetic nanocomposite hydrogels based on chitosan prepared by gamma rays. *Carbohydr. Polym.* 283, 119149. doi:10.1016/j.carbpol.2022.119149

Almeida, C. A. P., dos Santos, A., Jaerger, S., Debacher, N. A., and Hankins, N. P. (2010). Mineral waste from coal mining for removal of astrazon red dye from aqueous solutions. *Desalination* 264, 181–187. doi:10.1016/j.desal.2010.09.023

Arellano-Cardenas, S., Lopez-Cortez, S., Cornejo-Mazon, M., and Mares-Gutierrez, J. C. (2013). Study of malachite green adsorption by organically modified clay using a batch method. *Appl. Surf. Sci.* 280, 74–78. doi:10.1016/j.apsusc.2013.04.097

Bhattacharyya, K. G., SenGupta, S., and Sarma, G. K. (2014). Interactions of the dye, Rhodamine B with kaolinite and montmorillonite in water. *Appl. Clay Sci.* 99, 7–17. doi:10.1016/j.clay.2014.07.012

Brini, L., Hsini, A., Naciri, Y., Bouziani, A., Ajmal, Z., H'Maida, K., et al. (2021). Synthesis and characterization of arginine-doped heliotrope leaves with high clean-up capacity for crystal violet dye from aqueous media. *Water Sci. Technol.* 84, 2265–2277. doi:10.2166/wst.2021.446

Cengiz, S., Tanrikulu, F., and Aksu, S. (2012). An alternative source of adsorbent for the removal of dyes from textile waters: *Posidonia oceanica* (L.). *Chem. Eng. J.* 189-190, 32–40. doi:10.1016/j.cej.2012.02.015

Dadban Shahamat, Y., Masihpour, M., Borghei, P., and Hoda Rahmati, S. (2022). Removal of azo red-60 dye by advanced oxidation process O_3/UV from textile wastewaters using Box-Behnken design. *Inorg. Chem. Commun.* 143, 109785. doi:10.1016/j.inoche.2022.109785

Dehmani, Y., Khalki, O. E., Mezougane, H., and Abouarnadasse, S. (2021). Comparative study on adsorption of cationic dyes and phenol by natural clays. *Chem. Data Collect.* 33, 100674. doi:10.1016/j.cdc.2021.100674

Doğar, Ç., Gürses, A., Açıkyıldız, M., and Özkan, E. (2010). Thermodynamics and kinetic studies of biosorption of a basic dye from aqueous solution using green algae Ulothrix sp. *Colloids Surfaces B Biointerfaces* 76, 279–285. doi:10.1016/j.colsurfb.2009.11.004

Drumond Chequer, F. M., de Oliveira, G. A. R., Anastacio Ferraz, E. R., Carvalho, J., Boldrin Zanoni, M. V., and de Oliveir, D. P. (2013). "Textile dyes: Dyeing process and environmental impact," in *Eco-friendly textile dyeing and finishing*. Editor M. Gunay (France: InTech). doi:10.5772/53659

El-Ashtoukhy, E.-S. Z., and Amin, N. K. (2010). Removal of acid green dye 50 from wastewater by anodic oxidation and electrocoagulation-A comparative study. *J. Hazard. Mater.* 179, 113–119. doi:10.1016/j.jhazmat.2010.02.066

Fahoul, Y., Tanji, K., Zouheir, M., Mrabet, I. E., Naciri, Y., Hsini, A., et al. (2022). Novel River Sediment@ZnO Co nanocomposite for photocatalytic degradation and COD reduction of crystal violet under visible light. *J. Mol. Struct.* 1253, 132298. doi:10.1016/j.molstruc.2021.132298

Fu, N., and Ren, X. (2020). Synthesis of double-shell hollow TiO_2@zif-8 nanoparticles with enhanced photocatalytic activities. *Front. Chem.* 8, 578847. doi:10.3389/fchem.2020.578847

Gamoudi, S., and Srasra, E. (2019). Adsorption of organic dyes by HDPy+-modified clay: Effect of molecular structure on the adsorption. *J. Mol. Struct.* 1193, 522–531. doi:10.1016/j.molstruc.2019.05.055

Gul, R., Sharma, P., Kumar, R., Umar, A., Ibrahim, A. A., Alhamami, M. A. M., et al. (2023). A sustainable approach to the degradation of dyes by fungal species isolated from industrial wastewaters: Performance, parametric optimization, kinetics and degradation mechanism. *Environ. Res.* 216, 114407. doi:10.1016/j.envres.2022.114407

Gul, S., Kanwal, M., Qazi, R. A., Gul, H., Khattak, R., Khan, M. S., et al. (2022). Efficient removal of methyl red dye by using bark of hopbush. *Water* 14, 2831. doi:10.3390/w14182831

Gupta, V., Shrivastava, A., and Jain, N. (2001). Biosorption of chromium (VI) from aqueous solutions by green algae spirogyra species. *Water Res.* 35 (17), 4079–4085. doi:10.1016/s0043-1354(01)00138-5

Gürses, A., Doğar, C., Yalçın, M., Açıkyıldız, M., Bayrak, R., and Karaca, S. (2006). The adsorption kinetics of the cationic dye, methylene blue, onto clay. *J. Hazard. Mater.* 131, 217–228. doi:10.1016/j.jhazmat.2005.09.036

Gürses, A., Karaca, S., Açikyildiz, M., and Ejder (Korucu), M. (2009). Thermodynamics and mechanism of cetyltrimethylammonium adsorption onto clayey soil from aqueous solutions. *Chem. Eng. J.* 147, 194–201. doi:10.1016/j.cej.2008.07.001

Gürses, A., Karaca, S., Doğar, Ç., Bayrak, R., Açıkyıldız, M., and Yalçın, M. (2004). Determination of adsorptive properties of clay/water system: Methylene blue sorption. *J. Colloid Interface Sci.* 269, 310–314. doi:10.1016/j.jcis.2003.09.004

Hsini, A., Naciri, Y., Bouziani, A., Aarab, N., Essekri, A., Imgharn, A., et al. (2021). Polyaniline coated tungsten trioxide as an effective adsorbent for the removal of orange G dye from aqueous media. *RSC Adv.* 11, 31272–31283. doi:10.1039/D1RA04135E

Hussaan, M., AmnaJaved, M. T., Akram, M. S., and Ali, S. (2021). "Physiological and molecular basis of bioremediation of micropollutants," in *Handbook of bioremediation* (Netherlands: Elsevier), 447–464. doi:10.1016/B978-0-12-819382-2.00028-4

Hussain, T., and Wahab, A. (2018). A critical review of the current water conservation practices in textile wet processing. *J. Clean. Prod.* 198, 806–819. doi:10.1016/j.jclepro.2018.07.051

Ihaddaden, S., Aberkane, D., Boukerroui, A., and Robert, D. (2022). Removal of methylene blue (basic dye) by coagulation-flocculation with biomaterials (bentonite and *Opuntia ficus indica*). *J. Water Process Eng.* 49, 102952. doi:10.1016/j.jwpe.2022.102952

Imgharn, A., Aarab, N., Hsini, A., Naciri, Y., Elhoudi, M., Haki, M. A., et al. (2022). Application of calcium alginate-PANI@sawdust wood hydrogel bio-beads for the removal of orange G dye from aqueous solution. *Environ. Sci. Pollut. Res.* 29, 60259–60268. doi:10.1007/s11356-022-20162-9

Imgharn, A., Laabd, M., Naciri, Y., Hsini, A., Mahir, F.-Z., Zouggari, H., et al. (2023). Insights into the performance and mechanism of PANI@Hydroxapatite-Montmorillonite for hexavalent chromium Cr (VI) detoxification. *Surfaces Interfaces* 36, 102568. doi:10.1016/j.surfin.2022.102568

Jawad, A. H., and Abdulhameed, A. S. (2020). Mesoporous Iraqi red kaolin clay as an efficient adsorbent for methylene blue dye: Adsorption kinetic, isotherm and mechanism study. *Surfaces Interfaces* 18, 100422. doi:10.1016/j.surfin.2019.100422

Jinisha, R., Gandhimathi, R., Ramesh, S. T., Nidheesh, P. V., and Velmathi, S. (2018). Removal of rhodamine B dye from aqueous solution by electro-Fenton process using iron-doped mesoporous silica as a heterogeneous catalyst. *Chemosphere* 200, 446–454. doi:10.1016/j.chemosphere.2018.02.117

Joseph, J., Radhakrishnan, R. C., Johnson, J. K., Joy, S. P., and Thomas, J. (2020). Ion-exchange mediated removal of cationic dye-stuffs from water using ammonium phosphomolybdate. *Mater. Chem. Phys.* 242, 122488. doi:10.1016/j.matchemphys.2019.122488

Karagozoglu, B., Tasdemir, M., Demirbas, E., and Kobya, M. (2007). The adsorption of basic dye (Astrazon Blue FGRL) from aqueous solutions onto sepiolite, fly ash and apricot shell activated carbon: Kinetic and equilibrium studies. *J. Hazard. Mater.* 147, 297–306. doi:10.1016/j.jhazmat.2007.01.003

Kim, S.-H., Kim, D.-S., Moradi, H., Chang, Y.-Y., and Yang, J.-K. (2023). Highly porous biobased graphene-like carbon adsorbent for dye removal: Preparation, adsorption mechanisms and optimization. *J. Environ. Chem. Eng.* 11, 109278. doi:10.1016/j.jece.2023.109278

Loutfi, M., Mariouch, R., Mariouch, I., Belfaquir, M., and ElYoubi, M. S. (2023). Adsorption of methylene blue dye from aqueous solutions onto natural clay: Equilibrium and kinetic studies. *Mater. Today Proc.* 72, 3638–3643. doi:10.1016/j.matpr.2022.08.412

Martorell, M. M., Pajot, H. F., and de Figueroa, L. I. C. (2012). Dye-decolourizing yeasts isolated from Las Yungas rainforest. Dye assimilation and removal used as selection criteria. *Int. Biodeterior. Biodegrad.* 66, 25–32. doi:10.1016/j.ibiod.2011.10.005

Marungrueng, K., and Pavasant, P. (2006). Removal of basic dye (Astrazon Blue FGRL) using macroalga *Caulerpa lentillifera*. *J. Environ. Manag.* 78, 268–274. doi:10.1016/j.jenvman.2005.04.022

Mo, Y., Du, M., Yuan, T., Liu, M., Wang, H., He, B., et al. (2020). Enhanced anodic oxidation and energy saving for dye removal by integrating O_2-reducing biocathode into electrocatalytic reactor. *Chemosphere* 252, 126460. doi:10.1016/j.chemosphere.2020.126460

Naciri, Y., Hsini, A., Bouziani, A., Tanji, K., El Ibrahimi, B., Ghazzal, M. N., et al. (2022). Z-Scheme WO3/PANI heterojunctions with enhanced photocatalytic activity under visible light: A depth experimental and dft studies. *Chemosphere* 292, 133468. doi:10.1016/j.chemosphere.2021.133468

Nataraj, S. K., Hosamani, K. M., and Aminabhavi, T. M. (2009). Nanofiltration and reverse osmosis thin film composite membrane module for the removal of dye and salts from the simulated mixtures. *Desalination* 249, 12–17. doi:10.1016/j.desal.2009.06.008

Önal, M., and Sarıkaya, Y. (2007). Thermal behavior of a bentonite. *Journal of Thermal Analysis and Calorimetry.* 90 (1), 167–172. doi:10.1007/s10973-005-7799-9

Pimol, P., Khanidtha, M., and Prasert, P. (2008). Influence of particle size and salinity on adsorption of basic dyes by agricultural waste: Dried seagrape (*Caulerpa lentillifera*). *J. Environ. Sci.* 20, 760–768. doi:10.1016/S1001-0742(08)62124-5

Rápó, E., and Tonk, S. (2021). Factors affecting synthetic dye adsorption; desorption studies: A review of results from the last five years (2017-2021). *Molecules* 26, 5419. doi:10.3390/molecules26175419

Riegas-Villalobos, A., Martínez-Morales, F., Tinoco-Valencia, R., Serrano-Carreón, L., Bertrand, B., and Trejo-Hernández, M. R. (2020). Efficient removal of azo-dye Orange II by fungal biomass absorption and laccase enzymatic treatment. *3 Biotech.* 10, 146. doi:10.1007/s13205-020-2150-5

Santos, S. C. R., and Boaventura, R. A. R. (2008). Adsorption modelling of textile dyes by sepiolite. *Appl. Clay Sci.* 42, 137–145. doi:10.1016/j.clay.2008.01.002

Srinivasan, S., Bankole, P. O., and Sadasivam, S. K. (2022). Biodecolorization and degradation of textile azo dyes using *Lysinibacillus sphaericus* MTCC 9523. *Front. Environ. Sci.* 10, 990855. doi:10.3389/fenvs.2022.990855

Stawiński, W., Węgrzyn, A., Dańko, T., Freitas, O., Figueiredo, S., and Chmielarz, L. (2017). Acid-base treated vermiculite as high performance adsorbent: Insights into the mechanism of cationic dyes adsorption, regeneration, recyclability and stability studies. *Chemosphere* 173, 107–115. doi:10.1016/j.chemosphere.2017.01.039

Tanji, K., Zouheir, M., Hachhach, M., Ahmoum, H., Jellal, I., Masaoudi, H. E., et al. (2021). Design and simulation of a photocatalysis reactor for rhodamine B degradation using cobalt-doped ZnO film. *Reac Kinet. Mech. Cat.* 134, 1017–1038. doi:10.1007/s11144-021-02116-3

Wang, X., Jiang, J., and Gao, W. (2022). Reviewing textile wastewater produced by industries: Characteristics, environmental impacts, and treatment strategies. *Water Sci. Technol.* 85, 2076–2096. doi:10.2166/wst.2022.088

Yaseen, D. A., and Scholz, M. (2019). Textile dye wastewater characteristics and constituents of synthetic effluents: A critical review. *Int. J. Environ. Sci. Technol.* 16, 1193–1226. doi:10.1007/s13762-018-2130-z

Yesilada, O., Cing, S., and Asma, D. (2002). Decolourisation of the textile dye Astrazon Red FBL by *Funalia trogii* pellets. *Bioresour. Technol.* 81, 155–157. doi:10.1016/S0960-8524(01)00117-1

Zhang, H., Zhang, K., Gao, M., An, Z., Tang, C., and Yan, X. (2022). Degradation efficiency of the azo dye acid orange 2 and microbial community characteristics in a rotating algal biofilm reactor. *J. Water Process Eng.* 50, 103233. doi:10.1016/j.jwpe.2022.103233

Zhao, J., Liu, H., Xue, P., Tian, S., Sun, S., and Lv, X. (2021). Highly-efficient PVDF adsorptive membrane filtration based on chitosan@CNTs-COOH simultaneous removal of anionic and cationic dyes. *Carbohydr. Polym.* 274, 118664. doi:10.1016/j.carbpol.2021.118664